The rain is askew: Two idealized models relating vertical velocity and precipitation distributions in a warming world

Angeline G. Pendergrass*

National Center for Atmospheric Research, Boulder, Colorado, USA.

Edwin P. Gerber

Center for Atmosphere and Ocean Sciences, Courant Institute, New York University, New York, New York

**Corresponding author address:* Angeline G. Pendergrass, P.O. Box 3000, Boulder, CO 80307.

The National Center for Atmospheric Research is sponsored by the National Science Foundation.

Current affiliation: CIRES, University of Colorado - Boulder.

E-mail: apgrass@ucar.edu

ABSTRACT

As the planet warms, climate models predict that rain will become heavier but less frequent, and that the circulation will weaken. Here, two heuristic models relating moisture, vertical velocity, and rainfall distributions are developed, one in which the distribution of vertical velocity is prescribed and another in which it is predicted. These models are used to explore the response to warming and moistening, changes in the circulation, atmospheric energy budget, and stability. Some key assumptions of the models include that relative humidity is fixed within and between climate states and that stability is constant within each climate state. The first model shows that an increase in skewness of the vertical velocity distribution is crucial for capturing salient characteristics of the changing distribution of rain, including the muted rate of mean precipitation increase relative to extremes and the decrease in the total number or area of rain events. The second model suggests that this increase in the skewness of the vertical velocity arises from the asymmetric impact of latent heating on vertical motion.

1. Introduction

Changes in rain are inexorably tied to changes in atmospheric circulation. In response to global warming, climate model projections show an increase in global-mean precipitation, the rate of which is in balance with the change in atmospheric radiative cooling (O'Gorman et al. 2012; Pendergrass and Hartmann 2014a). This rate of increase, 1-3% per degree of warming across climate models, is smaller than the rate of increase of moisture in the atmosphere, which roughly follows saturation vapor pressure at $\sim$7%K^{-1} (Held and Soden 2006). The difference between the rates of increase of moisture and precipitation with warming imply a slowing of the atmospheric overturning circulation (Betts 1998). The weakening circulation in climate model projections manifests as a decrease in spatial variance of convective mass flux (Held and Soden 2006) and the Walker circulation (the anti-symmetric component of variance of 500 hPa vertical velocity in the tropics, Vecchi and Soden 2007).

Along with changes in circulation, climate models project substantial changes in the distribution of rainfall, as shown in Fig. 1. The rain frequency distribution (Fig. 1a) shows how often it rains at any particular rain rate. It is displayed on a logarithmic rain-rate scale in order to accommodate the full range of rain rates that can be encountered, which encompasses orders of magnitude. The rain amount distribution (Fig. 1b) shows how much rain falls at a particular rain rate. These calculations are based on the mean of the Coupled Model Intercomparison Project version 5 (CMIP5, Taylor et al. 2012) models and are described in more detail in Pendergrass and Hartmann (2014b). Figures 1c,d show the multi-model mean changes in the rain frequency and rain amount distributions in response to a doubling of carbon dioxide in a scenario where carbon dioxide concentrations increase by 1% each year. The rain frequency response to warming (Fig. 1c) is an increase in days with heavy rain, a larger decrease in days with moderate rain, a small (statistically insignificant) increase in days with light rain, and a small (statistically significant) increase in the number of dry days (noted at the top left of the panel). The rain amount response (Fig. 1d) is an increase in rain falling at heavy rain rates and a smaller decrease in rain falling at moderate rain rates, comprising an increase in the total amount of precipitation.

Pendergrass and Hartmann (2014c) found that these changes in the distribution of rainfall in response to warming (as well as those arising in response to El Niño and La Nina phases of ENSO) in models can be well described by two empirically-derived patterns, denoted the "shift" and "increase" modes, which are illustrated in Fig. 2. Each mode describes a simple adjustment to the climatological distribution of rain. A combination of the shift and increase modes (chosen with an algorithm to optimize the fit to the change in rain amount distribution) captures most of the response in most climate model simulations of global warming, and the entire change in some models.

The "increase" mode (Fig. 2a,b) characterizes an increase in the frequency of rain by the same fraction at all rain rates. The bell shape of this mode simply follows the climatological distribution of rain frequency. While the change in rain amount is characterized by a similar bell-shaped pattern, it occurs at higher rain rates (Fig. 2b). The total amount of rain is the product of the rain frequency and rain rate, such that an increase in rain frequency at higher rain rates has a larger impact on the total precipitation than it does at lower rain rates. An increase in rain frequency implies a reduction in the number of dry days. In the global mean, it rains about half of the time, such that a one percent increase at all rain rates is associated with a one-half percent reduction in dry days.

The "shift" mode (Fig. 2c,d) characterizes a movement of the distribution of rain to higher rain rates, but with no net increase in the total rain amount. It is defined as a shift of the rain amount distribution (Fig. 2d); the corresponding change in the rain frequency distribution can also be obtained (Fig. 2c). A larger decrease in the frequency of light rain events is needed to offset the smaller increase in the frequency of strong rain events on total precipitation, hence the shift mode is associated with an increase in the number of dry days. For a one percent increase in the shift mode, the total number of dry days increases by about one-half of a percent.

Pendergrass and Hartmann (2014b) determined that the shift and increase mode magnitudes that optimally capture the change in the multi-model mean rain amount distribution in Fig. 1d is a shift mode of 3.3 $\%K^{-1}$ along with an increase mode of 0.9 $\%K^{-1}$. Figure 2e,f show the change in rain frequency and amount distributions for this combination of shift and increase modes. The response of the shift mode is larger than the increase mode, such that there is a modest increase in the frequency of dry days.

Not all of the change in the distribution of rain in climate models is captured by the shift and increase modes. Pendergrass and Hartmann (2014c) identified two additional aspects of the changing distribution of rain common to many models: the light rain mode and the extreme mode. The light rain mode is the small increase in rain frequency just below 1 mm d^{-1} visible in Fig. 1c, also evident in Lau et al. (2013). The extreme mode represents additional increases in rain at the heaviest rain rates, beyond what is captured by the shift and increase modes. It is crucial for capturing the response of extreme precipitation to warming.

Changes in moisture, circulation, and the distribution of rain in response to warming are related. Indeed, the changes in the intensity of extreme rain events in climate model projections of global warming can be linearly related to changes in moisture and vertical velocity in most models and regions (Emori and Brown 2005; O'Gorman and Schneider 2009; Chou et al. 2012). This motivates us to consider whether we can understand the changing distribution of rain in terms of the changes in moisture and vertical velocity distributions, constituting a physically based, rather than empirically derived, approach.

One might assume that changes in the distribution of rain are complex. The distribution of rain (particularly the global distribution) is generated by a number of different types of precipitating systems, each of which is driven by somewhat different mechanisms and might respond differently to external forcing. For example, it would not be surprising if midlatitude cyclones and tropical convection responded differently to global warming. On the other hand, we expect many aspects of the response to warming to be fairly straightforward: warming along with moistening at a relative humidity that stays constant on surfaces of constant temperature (Romps 2014).

In this study, we approach the relationships among changes in moisture, vertical velocity, and rain by examining the response to straightforward changes of simple statistical distributions. We develop two heuristic models that predict the distribution of rain from moisture and vertical velocity distributions. We will see that despite the potential for complexity among these relationships, we can recover many aspects of the changes in rainfall and vertical velocity we see in climate models in an idealized setting.

In Section 2, we introduce the first model, in which distributions of moisture and vertical velocity are prescribed. We use the model to explore how the distribution of rain responds to warming and moistening, and to changes in the strength and asymmetry (or skewness) of the vertical velocity distribution. Then, in Section 3, we introduce a second model that predicts the vertical velocity distribution in order to understand its changes in concert with those of the distribution of rain. In Section 4, we show that climate model simulations also have increasing skewness of vertical velocity with warming. Finally, we consider the implications of the increasing skewness of vertical velocity on convective area in Section 5 and conclude our study in Section 6.

2. The first model: Prescribed vertical velocity

We know rain is a result of very complex processes, many of which are parameterized rather than explicitly modeled in climate models. At the most basic level, rain is regulated by two processes: (1) the moisture content, which is tied to the temperature structure, assuming constant relative humidity, and (2) the magnitude of upward vertical velocity. Instead of considering variability in space, consider a distribution that captures the structure of all regions globally. Furthermore, neglect concerns about the vertical structure of the motion or the structure of the atmosphere, and consider only the vertical flux of moisture through the cloud base.

The key – and gross – simplification of this model is that we will assume that the vertical velocity is *independent* of the temperature and moisture content, so we can model these as two independent distributions. We know this is not the case – upward velocity is often driven by convection, which occurs where surface temperature is warm – but for now we will see what insight can be gleaned with this assumption.

a. Model description

Our first model is driven by two prescribed, independent, Gaussian (normal) distributions: one for temperature, $N(\overline{T}, \sigma_T)$, where $\overline{T}$ is the mean temperature and σ_T is width of the temperature distribution, and another for vertical velocity, $N(\overline{w}, \sigma_w)$, where $\overline{w}$ is the mean vertical velocity (equal to zero when mass is conserved) and σ_w is the width of the w distribution. The temperature distribution, with the assumption of constant relative humidity, in turn gives us the moisture distribution. We calculate moisture q,

$$q(T) = q_0 e^{0.07T}, \tag{1}$$

where q_0 is chosen so that $q(T)$ is equal to its Clausius-Clapeyron value at $T = 287$ K. This equation is very similar to Clausius-Clapeyron, except that here $dq/dT = 7$ %K^{-1} exactly. The implied relative humidity is fixed at 100%. The choice of 100% relative humidity is arbitrary, but any non-zero choice that is held constant will result in the same behavior.

We suppose that it rains whenever vertical velocity w is positive (upward), with a rain rate equal to the product of the moisture, vertical velocity, and air density ρ_a (held constant at 1.225 kg m^{-3}, its value at sea level and 15°C),

$$r(q,w) = \begin{cases} \rho_a w q, & w > 0 \\ 0, & w \leq 0. \end{cases} \tag{2}$$

This is analogous to saying that the rain rate is equal to the flux of moisture across the cloud base. While this is a gross simplification, it would hold if the column were saturated and the temperature structure fixed, and the air was lifted to a level where the saturation specific humidity is effectively zero. In this limit, any moisture advected upward will lead to supersaturation and rain from above. Neglecting the impact of condensation on the temperature is a similarly coarse approximation as our assumption that the temperature and vertical velocity are independent.

The rain frequency distribution is obtained by integrating across the distributions of T (which determines q by Eqn. 1) and w,

$$p(r) = \int_0^{\infty} \int_{-\infty}^{\infty} \int_{-\infty}^{\infty} \delta\left(r - \rho_a w q\right)\ p(T)\ p(w)\ dT\ dw\ dr, \tag{3}$$

where $p(T)$ and $p(w)$ are Gaussian probability density functions and δ is a Dirac delta function. The rain amount distribution is then,

$$P(r) = r\, p(r). \tag{4}$$

In practice, $p(r)$ and $P(r)$ are computed over a discrete set of bins. Because the rain rate varies over several orders of magnitude, the bins are spaced evenly on a logarithmic scale for proper sampling; the bin width defined in logarithmic space is $\Delta lnr = \Delta r_i / r_i$, where r_i is the rain rate and Δr_i is the linear bin width for the ith bin. We then work with the frequency of rain events corresponding to each bin, $p(r_i)\Delta r_i$. To maintain the property that the area under the displayed distribution curves accurately represents the contribution of each rain rate to the total integral when displayed on a logarithmic scale, our plots show $r_i p(r_i) = p(r_i)\Delta r_i / \Delta lnr$.

Lastly, we must specify the parameters governing the temperature and vertical velocity distributions, which are listed in Table 1 for reference. For temperature (shown in Fig. 3a) we take $\overline{T}$ to be 287 K and its standard deviation $\sigma_T = 16$ K, both chosen to match the surface air temperature distribution in a climate model. The vertical velocity distribution (shown in Fig. 3b) must have a mean $\overline{w} = 0$ if mass is to be conserved. Given the temperature distribution above, the standard deviation of w will ultimately set the total precipitation. Thus we sought to constrain its value so as to capture the total precipitation in climate models and observational datasets (see Pendergrass and Hartmann 2014c), while at the same time being consistent with the vertical velocity distribution in climate models. Studies such as Emori and Brown (2005) show that rain frequency changes are linearly related to changes in moisture and 500 hPa vertical velocity in many climate models for most regions. While vertical velocity at cloud base rather than 500 hPa would be more closely physically related to our conceptual model, it is not archived for these climate model integrations.

The rain frequency distribution (shown in Fig. 3c) is calculated numerically following the description in Appendix A. It is dry exactly 50% of the time, since the vertical velocity distribution is symmetric about zero. The peak of the rain frequency distribution occurs at just under 10 mm d^{-1}. The rain amount distribution (Fig. 3d) shows how much rain falls in each rain rate bin. The peak of the rain amount distribution occurs at a rain rate about an order of magnitude larger than for the rain frequency distribution.

These distributions resemble those in observational datasets and climate models to the correct order of magnitude – compare to Fig. 1a,b and Pendergrass and Hartmann (2014c) – despite the crude assumptions of our model. The main deficiency of our model compared to climate models is a lack of precipitation at light rain rates, and a corresponding overestimation of dry-day frequency. However, climate models underestimate the dry-day frequency by about a factor of two compared to GPCP 1DD and TRMM 3B42 merged satellite-gauge gridded daily observational datasets (Pendergrass and Hartmann 2014c). The implications of this discrepancy on the rain amount distribution are nonetheless small because light rain contributes less than heavy rain does to the total precipitation, so that distribution of rain amount appears better than rain frequency qualitatively (compare Figs. 1b and 3d).

The goal in developing this toy model is to explore what happens in response to perturbations: warming and moistening, weakening of the circulation, and introducing skewness to the vertical velocity distribution. We consider these next.

b. Response to warming and moistening

We approximate warming by simply shifting the mean of the temperature distribution $\overline{T}$ 1 K higher. We keep σ_T constant, assuming no change in the variance of temperature. The moisture distribution adjusts accordingly. We maintain the same w distribution and calculate the distribution of rain in the warmed climate. The difference between the distributions of rain frequency and amount in the warmed and initial climates are shown in Fig. 4a-c. There is no change in the total frequency of rain, and the total amount of rainfall increases by 7 $\%\mathrm{K}^{-1}$, exactly following the change in moisture.

The rainfall distribution response to warming is equivalent to moving the rain frequency distribution to the right by exactly 7 $\%\mathrm{K}^{-1}$, or having equal shift and increase modes of 7 $\%\mathrm{K}^{-1}$ (the fitted shift and increase modes are listed in Table 2), as in Fig. 2g,h. In contrast to this warming experiment, in climate model simulations of global warming the shift mode response is larger than that of the increase mode, and total precipitation increases more slowly than moisture. This exposes a flaw: circulation also adjusts to changes in climate, which is not captured by this first experiment. In climate model projections, circulation adjusts to satisfy the energetic constraints of the climate system, including the constraint that precipitation (in the global mean) can only increase as much as atmospheric radiative cooling and sensible heat flux allow (e.g. Allen and Ingram 2002).

c. Response to weakening circulation

A weakening of the atmospheric overturning circulation can be effected in our model by reducing the width of the vertical velocity distribution, σ_w. For our second experiment, we decrease the standard deviation of w by 4%, using the initial (not warmed) distribution of temperature and moisture. The change in the distribution of rain is shown in Fig. 4d-f.

Again, there is no change in the dry frequency, and the total amount of rainfall decreases by 4%, the same amount that we weakened the width of the vertical velocity distribution by. Decreasing the width of the vertical velocity distribution results in a shift of the rain frequency distribution to lower rain rates. In fact, narrowing the w distribution by 7% would exactly cancel the effect of warming by 1 K. We can understand this by considering Eqn. 2 or 3: warming by 1 K increases q by 7%, whereas widening the vertical velocity distribution increases w by 7%. The effect of either change on r is the same.

We have just seen that neither warming nor changing the strength of the circulation affects the dry frequency, or the symmetry between the rates of change of mean and extreme rainfall. Changes analogous to those we see in climate model simulations thus cannot result from either warming at constant relative humidity or weakening circulation alone. But what if the circulation becomes more asymmetric?

d. Response to changing skewness of vertical velocity

The first moment of the vertical velocity distribution, its mean, must be fixed at zero to maintain mass conservation. We have just seen that changing the second moment (standard deviation or variance) does not cause the changes in the distribution of rain that we see in climate models. We now turn to the third moment, skewness, which measures the asymmetry of a distribution. Skewness, a key quantity, is attended to more widely in the parts of atmospheric sciences dealing with turbulence, like boundary layer meteorology. It has also received some limited attention in climate recently. Monahan (2004) discusses skewness of low-level wind speed arising from surface drag. Luxford and Woollings (2012) discuss how skewness arises in geopotential height from kinematic fluctuations of the jet stream. Sardeshmukh et al. (2015) incorporate skewness into a non-linear model for atmospheric fields including precipitation. In particular, they highlight the skewness in the vertical velocity field.

Skewness can arise in vertical motion from the asymmetric effect of latent heating. To visualize this effect, picture a developing thunderstorm. The cumulus cloud grows because an updraft is heated when water vapor condenses, sustaining or even strengthening the updraft and eventually resulting in rainfall. Over the life of the thunderstorm, some of this rainfall will re-evaporate, but there will be a net latent heating of the atmosphere due to the formation of this thunderstorm equal to the amount of rainfall that reaches the ground. There is no corresponding effect of latent heating on subsiding air; it merely warms adiabatically as it sinks.

To incorporate skewness into the vertical velocity distribution, we draw w from a skew-normal distribution generated following Azzalini and Capitanio (1999), instead of from a normal distribution as before. A skew-normal distribution has three degrees of freedom which determine its mean, variance, and asymmetry. When the asymmetry is zero, the skew-normal distribution becomes normal. We adjust the skew-normal distribution so that the mean is always zero to maintain mass conservation, and we maintain a constant variance of the w distribution to eliminate the effects of changing circulation strength. The resulting distribution of w and the response in rain frequency and amount distributions to a 0.2 increase in skewness are shown in Fig. 4g-i.

The responses of the rain frequency and amount distributions to increasing skewness of the vertical velocity have some intriguing features. There is a notable decrease in the frequency of rain for moderate rain rates (Fig. 4h), but the total amount of rain remains essentially constant due to a slight increase in the frequency of higher rain rates (Fig. 4i). This strongly resembles the shift mode. The magnitude of the strongest updrafts also changes little. Increasing skewness without conserving the mean of w would increase the strength of the strongest updrafts, but the shift of the distribution to maintain mass continuity compensates for this.

To move toward the response of precipitation to global warming in climate models, we simultaneously warm and increase the skewness of the vertical velocity distribution, shown in Fig. 4j-l. The response of the rain frequency and amount distributions to warming and skewing has all the features seen in climate models: a decrease in the total rain frequency and in the frequency of rain falling at moderate rain rates, along with an increase in rain amount focused at the heaviest rain rates. Increasing the skewness of the vertical velocity distribution effects crucial components of the change. It decreases the total frequency of rain events, breaks the symmetry between the changes in mean and extreme rainfall, and allows us to change the magnitude of the shift mode without changing the increase mode.

To fully capture the changes we see in climate model simulations, we weaken the distribution of vertical velocity (decrease σ_w) while simultaneously increasing its skewness and increasing $\overline{T}$, shown in Fig. 4m-o. Here we see many of the same features as before, but now we also have the decrease in mean rainfall that arises from the weakening circulation, giving us shift and increase modes of roughly the same magnitude as we see in climate models.

To recap, we have shown that warming (increasing $\overline{T}$) results in shift and increase modes of equal magnitude, while increasing the skewness of the vertical velocity distribution produces the shift mode alone, allowing us to reproduce some salient features of the response of the rain distribution to warming projected by climate models. This motivates us to construct a model that predicts vertical velocity to understand how atmospheric energetic constraints lead to the increasing skewness of the vertical velocity distribution with warming.

3. The second model: Predicted vertical velocity

We know that precipitation is energetically constrained by total column heating and cooling. Thus, in this model we start with energetics. We prescribe a distribution of non-latent heating Q_n, which is the sum of radiative and sensible heating and the convergence of dry static energy flux in the atmospheric column (see Muller and O'Gorman 2011). In the time mean, $\overline{Q}_n$ balances the latent heating, and so relates to the total precipitation. In daily fields from the MPI-ESM-LR climate model, the width of the atmospheric radiative cooling distribution is small compared with that of the atmospheric column dry static energy flux convergence, so the standard deviation of the non-latent heating distribution, σ_{Q_n}, comes primarily from the convergence of the dry static energy flux. The distribution of $\overline{Q}_n$ thus captures both the impact of radiation and the transport of energy by the circulation.

a. Model description

Our goal is to predict the distribution of w, which will in turn give us the rainfall from Eqn. 2, as in our first model. We begin with the temperature and moisture distributions (again connected by the assumption of saturation, Fig. 5a), except that the tail of the temperature distribution is truncated at a maximum temperature, T_{max}, which in turn implies a maximum allowable moisture content. We then assume that the non-latent atmospheric column heating, Q_n (Fig. 5b), can be described by another independent Gaussian distribution. The sum of non-latent atmospheric column heating and latent heating from precipitation must be zero in the time mean to maintain energy conservation.

We calculate the distributions of vertical velocity and rain according to a form of the thermodynamic equation (inspired by Sobel and Bretherton 2000),

$$wS = Q_n + Q_l, \tag{5}$$

where the parameter S is a constant that converts energy to vertical motion. In Sobel and Bretherton (2000), S is a stability that varies in time and space, but here we assume it is a constant to maintain the mathematical simplicity of the model. Physically, this equation implies that the total atmospheric column heating (both latent, Q_l, and non-latent Q_n) exactly balances the energy required to move air (w) against stability S. This balance holds in the time mean in the real world, but here we enforce it at all times.

We calculate the latent heating Q_l from the moisture and vertical velocity when it is raining (as in the first model),

$$Q_l = L\rho_a w q, \tag{6}$$

where L is the latent heat of vaporization of water (which we hold constant at 2.5×10^{-6} J kg^{-1}, its value at 0°C) and ρ_a is the air density as in the first model. With substitution, we have an equation for vertical velocity,

$$w = \begin{cases} \frac{Q_n}{S}, & Q_n \leq 0 \\ \frac{Q_n}{S - L\rho_a q}, & Q_n > 0. \end{cases} \tag{7}$$

To conserve mass, the average vertical velocity must equal zero, as in the first model, and to conserve energy, the mean latent heating Q_l must be equal and opposite to the mean non-latent heating Q_n. These balances are effected by integral constraints based on Eqn. 5, derived in Appendix B.

The parameters we use are listed in Table 3. The mean of the non-latent atmospheric column heating is equal but opposite to the CMIP5 multi-model mean precipitation (88 W m^{-2}), and its standard deviation is dominated by variability in the dry static energy flux convergence on short time scales (following Muller and O'Gorman 2011); we choose a value similar to those we found in climate model integrations.

Truncating the temperature distribution is necessary to ensure that the denominator in Eqn. 7 never drops to or below zero, which would result in infinite w. T_{max} can be interpreted as an upper bound on SST, which is enforced by convection in the real world (Sud et al. 1999; Williams et al. 2009).

In addition to our choice of $\overline{Q}_n$, we also choose $\overline{T}$, σ_T, T_{max}, and σ_{Q_n} values that are plausibly realistic or comparable to calculations using daily data from the MPI-ESM-LR climate model. The other requirement to maintain a positive-definite denominator in Eqn. 7 is that S must be greater than $L\rho_a q(T_{max})$. In this way, the minimum possible choice of the parameter S is tied to T_{max}. With a realistic temperature and moisture distribution and a constant S, the minimum allowable value of S is much larger than observed values of static stability (see e.g., Juckes 2000).

The distributions of vertical velocity and rain produced by our model with the parameters listed in Table 3 are shown in Fig. 5c-e. As with the first model, the distributions of rain frequency and amount are qualitatively similar to observations and climate model simulations in terms of both the peak magnitudes and overall structure.

Most importantly, the model predicts a skewed distribution of w. To ensure that the skewness was not an artifact of the non-zero mean of the non-latent heating distribution, we specified $\overline{Q}_n = 0$ (thereby neglecting energy and mass balance) in an alternative calculation (not shown), and the positive skewness remained. Rather, the skewness arises from the asymmetry introduced by latent heating, as can be seen in Eqn. 7. Atmospheric column cooling ($Q_n < 0$) causes downward velocity, with a magnitude linearly related to Q_n, since S is constant. But atmospheric heating ($Q_n > 0$) induces upward motion and also condensation. The resulting latent heating effectively weakens the stability, and w is thus no longer simply proportional to Q_n, but grows super-linearly with Q_n.

b. Perturbations about the control climate

Here we explore the responses to the three parameters other than warming: mean non-latent heating $\overline{Q}_n$, the width of non-latent heating σ_{Q_n}, and stability S. To maintain mass and energy conservation, when one parameter changes, it must be compensated by a change in at least one other parameter. The amplitude of the parameter changes described in this section were chosen so they can be compared with the next set of experiments, where we warm by 3 K. This is a fairly linear regime where the results are not highly sensitive to the amplitude of the perturbations.

In the first experiment, we increase the magnitude of mean non-latent heating $\overline{Q}_n$ by 24 W m^{-2} to 113 W m^{-2} and balance it by widening the non-latent heating distribution (allowing σ_{Q_n} to increase by 27.5%, equivalent to increasing the strength of heat transport convergence). Details of how we carry out the variation of the parameters are discussed in Appendix A. The resulting distribution of vertical velocity and the changes in rain amount and rain frequency are shown in Fig. 6a-c. The vertical velocity distribution has widened, with no change in skewness. The rain frequency distribution shifts to heavier rain rates, with no change in the dry frequency, and thus no change in total rain frequency. The total amount of rainfall increases (to balance the increase in magnitude of non-latent heating), reflected in the response of the rain amount distribution.

Also included in Fig. 6c is the combined shift-plus-increase mode fitted to the rain amount response. The fitted shift-plus-increase response is colored orange (following the color scheme shown in Fig. 2), which corresponds to equal magnitudes of shift and increase modes. The magnitudes and error of the fit are listed in Table 2 (and are normalized by 3 K warming to compare with warming experiments, discussed next); the error is the magnitude of the response that the fitted shift-plus-increase fails to capture. The fitted shift mode is slightly bigger than the fitted increase mode, 11 versus 9 %K^{-1}.

The response of the vertical velocity and rainfall distributions is essentially the same response we would get from strengthening w in the first model (the opposite of the weakening w experiment in Fig. 4d-f), only here it is achieved in a way that is consistent with energy as well as mass balance. In this experiment, the magnitudes of vertical velocity and rain change, but the shape of their distributions, including of the fraction of events that are rain-producing updrafts, does not.

In the second experiment, we again increase the magnitude of mean non-latent heating, but now hold the width of the non-latent heating distribution constant and instead decrease stability S. We determine the decrease in S required to balance the increase in $\overline{Q}_n$ by linearizing the energy/mass balance equation about a perturbation in S, shown in Appendix C. A decrease of S by 19% is needed to maintain balance; the result is shown in Fig. 6d-f. Again we see strengthening of the vertical velocity distribution, but here we also see an increase in skewness of 38%. The change in rain frequency distribution has a shape that is similar to but not the same as in the previous experiment, because the symmetry is broken: there is an increase in the dry-day frequency by 0.4%, and thus a decrease in the total rain frequency. This change in symmetry arises from changing the mean of Q_n without changing its width, so that the fraction of non-latent heating events that are positive decreases (the positive w events and rainfall follow). The fitted shift-plus-increase mode to the rain amount response is colored magenta to correspond to a broken symmetry between the shift and increase modes.

In the third experiment, we narrow the distribution of non-latent heating by decreasing σ_{Q_n} by 23% and compensate it by decreasing S by 20%, holding $\overline{Q}_n$ constant (Fig. 6g-i). Here, there is negligible change in the width, or strength, of the vertical velocity distribution, but there is an increase in skewness which arises from strong (though still relatively infrequent) updrafts. The dry frequency increases, so there is an overall decrease in rain frequency, occurring mainly at moderate rain rates. At the same time, there is a slight increase in frequency at the heaviest rain rates and a larger (but still small) increase at light rain rates. The response of the rain amount distribution is dominated by the decrease at moderate rain rates and increase at heavy rain rates, which are in balance because the total rainfall does not change ($\overline{Q}_n$ is fixed). The shift-plus-increase mode is not a good fit for this response (light gray represents a poor fit of the shift-plus-increase mode).

The response of the vertical velocity distribution is a negligible change in width but an increase in skewness, which we can understand as follows. The narrowing Q_n distribution would weaken the vertical velocity distribution, but this is countered by the decrease in S, which strengthens it (see Eqn. 7). Meanwhile, decreasing σ_{Q_n} with no corresponding change in $\overline{Q}_n$ decreases the fraction of events that are updrafts. The w distribution must adjust so that the same total latent heating is achieved through fewer updrafts, which is accomplished by strengthening the strongest updrafts, increasing the skewness of vertical velocity.

The response of the rain frequency and amount distributions to changing σ_{Q_n} and S in Fig. 6g-i has some similarities to but also differences from the response to increasing skewness of w in the first model (Fig. 4g-i). The close fit by the shift mode of the rain amount response to increasing skewness in the first model indicates that the response is mostly just a movement of the rain amount distribution to higher rain rates. In contrast, in this model and experiment, the shift mode poorly captures the response. Despite that it is not captured by the shift and increase modes, the rain frequency and amount responses have interesting resemblances to the global warming response in climate models. One feature present here and in climate models that is not captured by the shift-plus-increase is the light rain mode identified in Pendergrass and Hartmann (2014b). The light rain mode is the small increase at light rain rates (around 1 mm d^{-1}) visible in Fig. 1c.

To summarize the effect of perturbing parameters other than temperature in this model: increasing $\overline{Q}_n$ increases the total amount of rainfall, while increasing σ_{Q_n} and decreasing S increase the magnitude of vertical velocity events and the intensity of rainfall. When the combination of parameters changes in such a way that the fraction of events that are updrafts changes, the skewness of the vertical velocity distribution also changes.

c. *Response to warming*

Next, we explore the response of the vertical velocity and rainfall distributions to warming. We increase $\overline{T}$ by 3 K (while allowing T_{max} to increase by the same amount). To maintain energy and mass balance while warming, we will begin by adjusting one other parameter at a time, considering three experiments in turn, shown in Fig. 7. These first experiments are designed to help us understand the model, and we will consider more realistic scenarios below.

In the first experiment, we balance warming by increasing S. Stability also changes in climate model simulations of global warming; specifically, dry static stability increases with warming in the tropics (e.g. Knutson and Manabe 1995) and subtropics and midlatitudes (e.g., Frierson 2006; Lu et al. 2007). We determine effects of changing T on energy and mass balance and the increase in S needed to balance it by linearizing Eqn. B4 for energy and mass balance about perturbations in S and T, shown in Appendix C. This linearization shows that one degree of warming is balanced by a 7% increase in stability, where the factor of 7% arises from the moistening associated with the warming. The distributions of vertical velocity and moisture that result from warming by 3 K and increasing stability by 21% are shown in Fig. 7a-c. The increased stability decreases the magnitude of vertical velocity for a given atmospheric column heating, so that the vertical velocity is weakened (its standard deviation decreases, as in Held and Soden 2006; Vecchi and Soden 2007) and the distribution of rainfall is exactly unchanged. The skewness of vertical velocity is also unchanged. In this model, the dry frequency is just the fraction of the time that the atmospheric column heating is negative; since atmospheric column heating does not change in this experiment, neither does the dry frequency. The tradeoff between warming and stability here is similar to the tradeoff between warming and the width of the vertical velocity distribution in our first model.

In the second experiment, we warm while increasing the magnitude of mean non-latent heating $\overline{Q}_n$ and holding all other parameters constant. Recall that $\overline{Q}_n$ controls the total precipitation. The resulting distributions of vertical velocity and rainfall are shown in Fig. 7d-f. The resulting vertical velocity distribution has no substantial change in width, but it does have increase in skewness. Similarly to the "narrow Q_n and decrease S" experiment in Fig. 6g-i, the increase in moisture and increase in mean Q_n have largely compensating effects on the vertical velocity distribution, except for a decrease in the total fraction of updrafts compared to downdrafts, resulting in an increase in skewness with little change in width of the w distribution. The response of the rain frequency distribution, on the other hand, is more similar to the increasing $\overline{Q}_n$ and decreasing S experiment. There is an increase in the dry frequency, and the rain amount response is captured by a shift mode that is slightly larger than the increase mode. Examination of Eqns. 2 and 7 reveals that this is possible because both experiments have the same change in Q_n, and decreasing S has the same effect on the denominator of Eqn. 7 as increasing q.

In the third experiment, warming is balanced by narrowing of the non-latent heating distribution (decreasing σ_{Q_n} or weakening the dry static energy flux convergence, Fig. 7g-i). In this experiment, the vertical velocity distribution weakens while the skewness increases. The skewness arises because of the decrease in upward frequency and adjustments to maintain mass as well as energy balance, while the weakening results from the weakening of the Q_n distribution. The rain frequency and amount distributions are very similar to the "narrowing Q_n and decreasing S" experiment with no warming.

In two final experiments, we emulate the changes seen in climate models: we warm and also increase the magnitude of non-latent atmospheric column heating $\overline{Q}_n$ by 1.1 W m^{-2} K^{-1}, which is the rate at which global-mean precipitation and clear-sky atmospheric radiative cooling increase in climate model projections of the response to transient carbon dioxide increase (Pendergrass and

Hartmann 2014a). This change in atmospheric radiative cooling includes both the temperature-mediated and direct effects of carbon dioxide. To maintain mass and energy balance, we allow a third parameter to change, and keep the fourth constant (first increasing S, and then decreasing σ_{Q_n}); these experiments are shown in Fig. 8. We examine each parameter change separately, but in at least one climate model simulation forced by a transient increase in carbon dioxide (with the MPI-ESM-LR model) both changes occur: S increases (by 1.7 %K^{-1} in the tropics) and σ_{Q_n} decreases (by 0.7 %K^{-1}).

First, we warm, increase mean Q_n, and allow S to increase. According to the linearizations about S and T in Appendix C, a change in stability of 6.0 %K^{-1} is needed to maintain energy and mass balance. This change in stability is slightly smaller than what was needed to balance warming alone (7 %K^{-1}, discussed in the first experiment above), due to the accompanying change in $\overline{Q}_n$. The result (shown in Fig. 8a-c) is a combination of the experiments where we warmed and varied mean Q_n and S separately. The vertical velocity distribution weakens and has a small increase in skewness. There is a modest increase in dry frequency, and a modest break in symmetry between the shift and increase modes (2.0 versus 1.6 %K^{-1}). This is not as large as the break in symmetry we see in climate models.

Finally, we warm, increase mean Q_n, and allow σ_{Q_n} to decrease by 6.2 %K^{-1}. This value of σ_{Q_n} change is need to restore energy and mass balance given the warming of 1 K and the increase in $\overline{Q}_n$ of 1.1 Wm^{2}K^{-1}, chosen following Appendix Ac. In Fig. 8d we see a weakening of the vertical velocity distribution and a larger increase in skewness than in Fig. 8a. Analogously to the warming and skewing experiment with the first model, the rain frequency and amount distribution responses (Fig. 8e,f) resemble the superposition of responses in previous experiments. The dry frequency increases, and the response of the rain frequency distribution has a decrease at moderate rain rates that is partially compensated by an increase at heavy rain rates. The rain frequency response strongly resembles the response we see in climate models (Fig. 1c), except that the light rain mode is absent. The rain amount distribution response is partially but not completely captured by the shift and increase modes, which reflects that it is the sum of a response that the shift-plus-increase captures (the response to warming while and increasing $|\overline{Q}_n|$) and one that it does not (the response to changing σ_{Q_n}). The fitted shift-plus-increase overestimates the decrease at moderate rain rates and underestimates the increase at heavy rain rates, reminiscent of the extreme mode identified in Pendergrass and Hartmann (2014b).

To summarize, in our second model, the atmosphere can respond in three ways to warming: (1) increasing the stability (S), which weakens the circulation (w) but has no effect on rain, (2) increasing the total precipitation ($\overline{Q}_n$), which drives an increase in skewness of w and of the intensity of the heaviest rainfall events, and (3) decreasing the width of the non-latent heating distribution (σ_{Q_n}), which leads to both a weakening of the circulation and increase in its skewness, and the accompanying increase in intensity of the heaviest rainfall events. In climate model projections of warming, energetic constraints require an increase in the total precipitation $\overline{Q}_n$.

In this simple model, if we warm and increase mean latent heating $\overline{Q}_n$, the stability S and/or width of the non-latent heating distribution σ_{Q_n} – which is intimately related to the circulation – must also change to maintain energy and mass balance. Any combination of these parameter changes results in: (1) a weakening of the circulations (i.e. of w), the essential conclusion of Vecchi and Soden (2007), (2) an increase in the skewness of w, and (3) an increase in intensity of the heaviest rain events (e.g., Trenberth 1999).

4. Comparison with the response to warming in climate models

The two heuristic models above show that increasing skewness of the vertical velocity distribution coincides with key characteristics of the changing distribution of rainfall that we see in climate models. Does skewness of the vertical velocity distribution increase with warming in climate models?

To address this question, we calculate statistics of daily-average 500 hPa pressure vertical velocity and their change in three warming experiments in the CMIP5 archive (Table 4). We calculate the area-weighted global-average moments from years 2006-2015 and 2090-2099 in the RCP8.5 scenario, and years 1-10 and 61-70 in the transient carbon dioxide increase 1pctCO2 scenario; these results can be compared with the fitted shift-plus-increase modes of the distribution of rain in Pendergrass and Hartmann (2014b). Trends in data can contaminate statistical measures of a distribution, so we also analyze the last 10 years of the CO_2 quadrupling experiment (abrupt4xco2), when the climate is as close to equilibrating as is available in the CMIP5 archive, and trends are as small as possible.

All climate model simulations have increasing skewness of vertical velocity, consistent with our expectations from the heuristic models along with the changing distribution of rain in climate models. The magnitude of increase in skewness varies widely across models, from less than 1 to 27 $\%K^{-1}$. Note that the models with the biggest increases in skewness (the GFDL-ESM and IPSL-CM5A models) also have a large extreme mode (Pendergrass and Hartmann 2014b). While we have touched on the extreme mode in our second heuristic model, much about it remains to be investigated.

The variance of vertical velocity decreases in all but one of the climate model simulations. Decreasing variance of vertical velocity at 500 hPa is consistent with Held and Soden (2006) and Vecchi and Soden (2007), though their metrics were slightly different from ours and the magnitude of changes shown here is smaller. Additionally, the change in vertical velocity strength at 500 hPa is expected to underestimate the weakening of the total vertical overturning circulation because the strongest motion is above 500 hPa and shifts upward with warming (Singh and O'Gorman 2012).

We include the changes in kurtosis in Table 4, the fourth moment of the distribution. Larger kurtosis corresponds to a fatter tail and a narrower peak of the distribution; a normal distribution has a kurtosis of 3 (e.g., DeCarlo 1997). In all climate models, kurtosis of vertical velocity is initially greater than Gaussian, and it increases with warming. Our second model predicts an increase in kurtosis along with the increases in skewness. Interestingly, the GFDL models have by far the largest increases in kurtosis with warming (they also have large extreme modes).

We are now in a position to reconcile the differing magnitudes of the shift and increase modes with warming that we see in climate model simulations. For the multi-model mean, moistening occurs at about 6-7 $\%\mathrm{K}^{-1}$ and global mean precipitation increases at 1.5 $\%\mathrm{K}^{-1}$. The multi-model mean rain amount response has an increase mode of 1 $\%\mathrm{K}^{-1}$ and a shift mode of 3.3 $\%\mathrm{K}^{-1}$. The MPI-ESM-LR model, whose response is best captured by the shift and increase modes, has an increase mode of 1.3 $\%\mathrm{K}^{-1}$ and a shift mode of 5.7 $\%\mathrm{K}^{-1}$.

We relate the shift and increase modes to changes in moisture and circulation as follows (and shown in Fig. 4 as well as listed in Table 2): moistening at 7 $\%\mathrm{K}^{-1}$ results in equal magnitudes of shift and increase modes. This is countered by a narrowing of the vertical velocity distribution that is not quite as large, bringing the net magnitudes of both the shift and increase modes down. Finally, an increase in skewness of the vertical velocity distribution results in a shift mode with no corresponding increase mode. The combination of these three changes results in a shift mode that is larger than the increase mode seen in the climate model response to warming.

While the heuristic models developed here capture some important aspects of the response of rainfall and vertical velocity to warming seen in climate models, the cost of its simplicity is the number of assumptions that must be made. Assumptions for our idealized relationship between moisture, vertical velocity and rain rate include: that all moisture is removed whenever there is upward motion, that the vertical structure of the atmosphere is fixed, and that relative humidity does not change. Our models do not accommodate any unresolved processes, parameterized in climate models, which can alter the relationship between rainfall and vertical velocity. This idealized framework also does not address the differing direct and temperature-mediated responses of precipitation and circulation to greenhouse gas forcing. Finally, aggregating over all locations and seasons convolves many different processes, and the relationships we explore here may not hold for all of them. Nonetheless, while we anticipate that our heuristic models do not capture the behavior of every relevant process that contributes to the responses of rainfall and vertical velocity to global warming, we think these models are useful for understanding a substantial portion of the response in many regions of most climate models.

5. Convective area

The spatial manifestation of the distribution of rain and vertical velocity is convective area, by which we mean the area with upward motion and the cloudiness and rainfall that accompany it. The fraction of time that vertical motion is upward and the fraction of time that it is raining in the heuristic models presented here is analogous to the fraction of the area in a domain where rain is occurring. The literature is currently unsettled about how the change in convective area and frequency of upward motion are expected to change with warming. Johnson and Xie (2010) argues that the convectively active fractional area of the tropics changes little relative to the area above an absolute SST threshold, which increases by 45% over the 21st century in the experiments they analyze, though this study focused on monthly mean precipitation, rather than daily data. In contrast, Vecchi and Soden (2007) report a decrease in the number of grid points with upward motion in GFDL-CM2.1 simulations of global warming in the tropics. Other recent studies focusing on monthly to seasonal mean precipitation find a decrease in the area of the ITCZ with warming (Neelin et al. 2003; Huang et al. 2013; Wodzicki and Rapp 2016). Byrne and Schneider (2016) examine the width of the ITCZ over a wide range of climates in a gray-radiation climate model and find different responses in different climate states. In CMIP5 model simulations, the frequency of dry days has a small but significant increase (see Fig. 1a or Pendergrass and Hartmann 2014b).

The heuristic models shown here reproduce the increase in dry frequency seen in the CMIP5 models and thus also the decrease in convective area. Figure 9 shows a schematic of the tropical overturning circulation to aid in interpreting its response to changes in the distribution of vertical velocity. The initial distribution has a region of ascent that is narrower than the region of descent, analogous to the circulation in the tropical atmosphere (Fig. 9a). Because the region of ascent is narrower and mass is conserved, the ascending motions are stronger than corresponding descending ones. Decreasing the standard deviation of the vertical velocity distribution decreases the magnitude of both upward and downward motion (weakening the circulation), with no change in area of either region (Fig. 9b). Increasing the skewness of vertical velocity increases the magnitude of upward motion while decreasing its area, and decreases the speed of descent while increasing its area (Fig. 9c). When the decrease in standard deviation and increasing skewness occur together, both contribute to weakening the descending motion, but they have competing effects on the magnitude of ascent, resulting in little change in updraft strength (Fig. 9d).

6. Conclusion

We have introduced two idealized models relating the distributions of rain and vertical velocity. In both models, temperature (and thus moisture, assuming constant relative humidity) is prescribed, and the distribution of rainfall is predicted. In the first model, the distribution of vertical velocity is also prescribed and can be varied; mass conservation is respected. In the second model, the distribution of non-latent atmospheric column heating is prescribed, the distribution of vertical velocity is predicted, and both mass and energy are conserved. Some key assumptions made by both models are that relative humidity is fixed within and between climate states and that stability is constant within each climate state.

Both of these models show that increasing skewness, or asymmetry, of the vertical velocity distribution is necessary to recover important characteristics of the changing distribution of rain with warming predicted by climate models: dry-day frequency increases, and extreme precipitation increases at a rate faster than the increase in mean precipitation. In the context of shift and increase modes of change of the distribution of rain, an increase in skewness is necessary to achieve the larger shift mode than increase mode seen in climate model projections. The second model, where the distribution of vertical velocity is predicted, shows how the asymmetric influence of latent heating creates skewness in the vertical velocity distribution. Experiments with this model show that this skewness increases in response to warming, along with the adjustments needed to maintain mass and energy balance. In addition to an increase in skewness, the standard deviation of the vertical velocity distribution also decreases, consistent with the weakening circulation found in climate model simulations of global warming.

The models developed here capture salient aspects of the changing distributions of rain and vertical velocity with simple thermodynamic relationships, implying that we do not need to resort to complex dynamical explanations for these aspects of the changing distribution of rain. The idealized relationships between the distributions of vertical velocity and precipitation explored here hopefully form a basis for understanding the richer and more complex interactions in climate models and in the real world.

Acknowledgments. We thank Clara Deser, Ben Sanderson, Brian Rose, Flavio Lehner, and two anonymous reviewers for their feedback. NCAR's Advanced Studies Program postdoctoral research fellowship provided funding for AGP. EPG acknowledges support from the National Science Foundation through grant AGS-1264195.

APPENDIX A

Numerical solutions

a. Normal and skew-normal distributions

We calculate the value of the normal distribution at points that are evenly spaced in percentile space, 5000 points for Model 1 and 10 000 for Model 2. For the temperature distribution, any values of $T > T_{max}$ are truncated. For making calculations over joint distributions (r over T/q and w in Model 1, r and w over Q_n and T/q in Model 2), we form a matrix over both distributions (of size 5000 x 5000 or 10 000 x 10 000[1]) and calculate the value at each point in the joint space.

Calculating the skew normal distribution is similar to a joint distribution because the algorithm of Azzalini and Capitanio (1999) calls for operating on two normal distributions. We start with normal distributions u_0 and v (5000 samples for each). To get a distribution with a shape parameter a (which is related to the skewness; when a is zero the distribution is normal, and we use $a > 0$ here), we calculate $u_1 = du_0 + \sqrt{(}1 - d^2)v$, where $d = a/\sqrt{(}1 + a^2)$ is a correlation related to the shape parameter. Then, the skewed distribution z is u_1 when $u_0 > 0$ and $-u_1$ otherwise. Finally, this 5000 x 5000 array is subsampled back to 5000 values by sorting them and keeping every 5000th one.

b. Frequency and amount distributions

We use logarithmically-spaced bins for the rain frequency and amount distributions, and choose 250 of them to obtain stable fits of the shift-plus-increase modes. Details of the calculation and

[1]With the introduction of T_{max}, we truncate a few values at the high end of the T/q distribution.

further examples of rain amount and rain frequency distributions can be found in Pendergrass and Hartmann (2014c). We use 50 linearly-spaced bins for $p(T)$, $p(Q_n)$, and $p(w)$, which are for display only.

c. Model 2 parameters

To calculate the parameters in the second model, there are two steps: the initial set up to find a balanced state and variation of parameters about this state.

To set up the model initially, the challenge is meeting energy and mass balance. We accomplish this numerically by specifying all parameters other than $\overline{Q}_n$, and then systematically solving for the value of $\overline{Q}_n$ that achieves energy and mass balance (Eqn. B4). First, we calculate the distribution of T from $\overline{T}$ and σ_T, truncating anything over T_{max}, and we calculate the associated q. Then with a choice of S, we calculate the LHS of the energy/mass balance equation (B in Appendix C). Finally, we use a specified value of σ_{Q_n}, and solve systematically for the value of $\overline{Q}_n$ that most closely results in mass/energy balance. We take a vector of 10 000 Gaussian values evenly spaced percentile-wise (call them y), and using the σ_{Q_n} value, calculate the RHS of the energy/mass balance equation that would result for each choice of $\overline{Q}_n = y\sigma_{Q_n}$. To vary parameters, new $\overline{T}$, σ_T, S, and σ_{Q_n} values can be manually chosen and a new $\overline{Q}_n$ found.

To find a new balanced state due to small variations in T and S around the initial balanced state, we use the linearizations in Appendix C. This is done in three different ways. Whenever possible, we use the linearization alone to find new values of T and S, or of the new LHS of the energy/mass balance equation. When necessary, we re-solve for a new $\overline{Q}_n$ that best meets energy/mass balance as we did to find the initial balanced $\overline{Q}_n$ value. Otherwise (e.g., when changing σ_{Q_n}), we iteratively choose parameter values (manually) until the energy/mass balance equation is satisfied again (to

4 decimal places). Once we have a new set of parameters, r, w, and their frequency and amount distributions $p(r)$, $P(r)$, and $p(w)$ are calculated once again.

APPENDIX B

Conservation of mass and energy

In this appendix, we derive the equation for mass and energy conservation of the model described in Section 3. In order to conserve mass, we must maintain an integral of vertical velocity over the entire distribution equal to zero,

$$\int_{-\infty}^{\infty} \int_{0}^{q_{max}} w \, p(q, Q_n) dq \, dQ_n = 0, \tag{B1}$$

where $p(q, Q_n)$ is the joint probability distribution function (pdf) of q and Q_n, and q_{max} is the maximum realized specific humidity, occurring at temperature T_{max}. In order to conserve energy, we enforce that the total latent heating must be balanced by the total non-latent heating,

$$\int_{-\infty}^{\infty} Q_n p(Q_n) dQ_n + \int_{-\infty}^{\infty} \int_{0}^{q_{max}} L \, r \, p(q, Q_n) dq \, dQ_n = 0, \tag{B2}$$

where $p(Q_n)$ is the pdf of non-latent heating Q_n.

Substituting Eqns. 2 and 5 into B2, separating regions of positive and negative Q_n, exploiting the independence of q and Q_n, and rearranging, we have,

$$\int_{0}^{q_{max}} \left[\frac{1}{1 - L\rho_a q / S} \right] p(q) dq = \frac{-\int_{-\infty}^{0} Q_n p(Q_n) dQ_n}{\int_{0}^{\infty} Q_n p(Q_n) dQ_n}. \tag{B3}$$

It is also possible to arrive at Eqn. B3 by starting from the mass conservation constraint (Eqn. B1), substituting Eqn. 5, exploiting the independence of q and Q_n, recognizing that $\int p(q)dq = 1$, and rearranging.

Following either path, we find that both the mass and energy constraints are met when,

$$E_q\left[\frac{1}{1 - L\rho_a q/S}\right] = \frac{-\int_{-\infty}^{0} Q_n p(Q_n) dQ_n}{\int_0^{\infty} Q_n p(Q_n) dQ_n}, \tag{B4}$$

where the expectation operator is defined as $E_x\left[f(x)\right] = \int_{-\infty}^{\infty} f(x)p(x)dx$.

APPENDIX C

Linearization of energy and mass balance about T and S

Here, we linearize the mass and energy conservation equation about its base state (the left hand side of Eqn. B4) to obtain its response to small changes in stability S and mean temperature $\overline{T}$. Along with new values of $\overline{Q}_n$ and σ_{Q_n} chosen by trial and error, we use this linearization to find new sets of parameters that satisfy energy and mass balance in the experiments described in Section 3b and c. To be concise, in this appendix we refer to the LHS of Eqn. B4 as B,

$$B = E_T\left[\frac{1}{1 - L\rho_a q(T)/S}\right]. \tag{C1}$$

a. Linearization in T

First, we linearize the LHS of Eqn. B4 to find its response to small changes in $\overline{T}$ and the associated moistening. We expand $T = \overline{T} + \Delta T = \overline{T}(1 + x)$, where $x = \Delta T/\overline{T} \ll 1$. Incorporating our moisture equation (1), we have,

$$B = \int_{-\infty}^{T_{max}} \frac{1}{1 - L\rho_a q_0 e^{0.07\overline{T}(1+x)}/S} p(T)dT. \tag{C2}$$

A first order Taylor expansion around B gives us,

$$B \approx B_0 + 0.07\ \Delta T\ B_1, \tag{C3}$$

where B_0 is the value of B evaluated at $T = \overline{T}$ and,

$$B_1 \equiv \int_0^{q_{max}} \frac{L\rho_a q/\overline{S}}{\left(1 - L\rho_a q/\overline{S}\right)^2}\ p(q)dq. \tag{C4}$$

This integral is readily evaluated numerically from a base q distribution.

b. Linearization in S

Next, we linearize Eqn. B4 to find the response to small changes in stability S. Expanding $S = \overline{S} + \Delta S = \overline{S}(1+x)$, where $x = \Delta S/\overline{S} \ll 1$, we have,

$$B = \int_0^{q_{max}} \frac{1}{1 - L\rho_a q/\overline{S}(1+x)}\ p(q)dq. \tag{C5}$$

Another Taylor expansion gives us,

$$B \approx B_0 - \frac{\Delta S}{\overline{S}} B_1. \tag{C6}$$

We can combine Eqns. C3 and C6 and solve for ΔS,

$$\Delta S = S\left(0.07\,\Delta T - \frac{B - B_0}{B_1}\right). \tag{C7}$$

Given a ΔT and possibly a new value of $\overline{Q}_n$ or σ_{Q_n} (which requires calculating a new value of B), we can solve for the ΔS that satisfies mass and energy balance.

References

Allen, M. R., and W. J. Ingram, 2002: Constraints on future changes in climate and the hydrologic cycle. *Nature*, **419 (6903)**, 224–232, doi:10.1038/nature01092.

Azzalini, A., and A. Capitanio, 1999: Statistical applications of the multivariate skew normal distribution. *J. Roy. Stat. Soc.: Ser. B (Stat. Methodol.)*, **61 (3)**, 579–602, doi:10.1111/1467-9868.00194.

Betts, A. K., 1998: Climate-convection feedbacks: Some further issues. *Clim. Change*, **39 (1)**, 35–38, doi:10.1023/A:1005323805826.

Byrne, M. P., and T. Schneider, 2016: Energetic constraints on the width of the intertropical convergence zone. *J. Climate*, doi:10.1175/JCLI-D-15-0767.1.

Chou, C., C.-A. Chen, P.-H. Tan, and K. T. Chen, 2012: Mechanisms for global warming impacts on precipitation frequency and intensity. *J. Climate*, **25 (9)**, 3291–3306, doi: 10.1175/JCLI-D-11-00239.1.

DeCarlo, L. T., 1997: On the meaning and use of kurtosis. *Psychol. Methods*, **2 (3)**, 292, doi: 10.1037/1082-989X.2.3.292.

Emori, S., and S. Brown, 2005: Dynamic and thermodynamic changes in mean and extreme precipitation under changed climate. *Geophys. Res. Lett.*, **32 (17)**, L17 706, doi:10.1029/2005GL023272.

Frierson, D. M., 2006: Robust increases in midlatitude static stability in simulations of global warming. *Geophys. Res. Lett.*, **33 (24)**, doi:10.1029/2006GL027504.

Held, I. M., and B. J. Soden, 2006: Robust responses of the hydrological cycle to global warming. *J. Climate*, **19 (21)**, 5686–5699, doi:10.1175/JCLI3990.1.

Huang, P., S.-P. Xie, K. Hu, G. Huang, and R. Huang, 2013: Patterns of the seasonal response of tropical rainfall to global warming. *Nat. Geosci.*, **6 (5)**, 357–361, doi:10.1038/ngeo1792.

Johnson, N. C., and S.-P. Xie, 2010: Changes in the sea surface temperature threshold for tropical convection. *Nat. Geosci.*, **3 (12)**, 842–845, doi:10.1038/ngeo1008.

Juckes, M., 2000: The static stability of the midlatitude troposphere: The relevance of moisture. *J. Atmos. Sci.*, **57 (18)**, 3050–3057.

Knutson, T. R., and S. Manabe, 1995: Time-mean response over the tropical Pacific to increased CO_2 in a coupled ocean-atmosphere model. *J. Climate*, **8 (9)**, 2181–2199.

Lau, W. K.-M., H.-T. Wu, and K.-M. Kim, 2013: A canonical response of precipitation characteristics to global warming from CMIP5 models. *Geophys. Res. Lett.*, **40 (12)**, 3163–3169, doi:10.1002/grl.50420.

Lu, J., G. A. Vecchi, and T. Reichler, 2007: Expansion of the Hadley cell under global warming. *Geophys. Res. Lett.*, **34 (6)**, doi:10.1029/2006GL028443.

Luxford, F., and T. Woollings, 2012: A simple kinematic source of skewness in atmospheric flow fields. *J. Atmos. Sci.*, **69 (2)**, 578–590, doi:10.1175/JAS-D-11-089.1.

Monahan, A. H., 2004: A simple model for the skewness of global sea surface winds. *J. Atmos. Sci.*, **61 (16)**, 2037–2049.

Muller, C. J., and P. A. O'Gorman, 2011: An energetic perspective on the regional response of precipitation to climate change. *Nat. Climate Change*, **1 (5)**, 266–271, doi:10.1038/nclimate1169.

Neelin, J., C. Chou, and H. Su, 2003: Tropical drought regions in global warming and El Niño teleconnections. *Geophys. Res. Lett.*, **30 (24)**, doi:10.1029/2003GL018625.

O'Gorman, P. A., R. P. Allan, M. P. Byrne, and M. Previdi, 2012: Energetic constraints on precipitation under climate change. *Surv. Geophys.*, **33 (3-4)**, 585–608, doi:10.1007/s10712-011-9159-6.

O'Gorman, P. A., and T. Schneider, 2009: The physical basis for increases in precipitation extremes in simulations of 21st-century climate change. *Proc. Natl. Acad. Sci. U. S. A.*, **106 (35)**, 14 773–14 777, doi:10.1073/pnas.0907610106.

Pendergrass, A., and D. Hartmann, 2014a: The atmospheric energy constraint on global-mean precipitation change. *J. Climate*, doi:JCLI-D-13-00163.1.

Pendergrass, A., and D. Hartmann, 2014b: Changes in the distribution of rain frequency and intensity in response to global warming. *J. Climate*, **27 (22)**, 8372–8383, doi:10.1175/JCLI-D-14-00183.1.

Pendergrass, A., and D. Hartmann, 2014c: Two modes of change of the distribution of rain. *J. Climate*, **27 (22)**, 8357–8371, doi:10.1175/JCLI-D-14-00182.1.

Romps, D. M., 2014: An analytical model for tropical relative humidity. *J. Climate*, **27 (19)**, 7432–7449, doi:10.1175/JCLI-D-14-00255.1.

Sardeshmukh, P. D., G. P. Compo, and C. Penland, 2015: Need for caution in interpreting extreme weather statistics. *J. Climate*, **28 (23)**, 9166–9187, doi:10.1175/JCLI-D-15-0020.1.

Singh, M. S., and P. A. O'Gorman, 2012: Upward shift of the atmospheric general circulation under global warming: Theory and simulations. *J. Climate*, **25 (23)**, 8259–8276, doi:10.1175/JCLI-D-11-00699.1.

Sobel, A. H., and C. S. Bretherton, 2000: Modeling tropical precipitation in a single column. *J. Climate*, **13 (24)**, 4378–4392.

Sud, Y., G. Walker, and K. Lau, 1999: Mechanisms regulating sea-surface temperatures and deep convection in the tropics. *Geophys. Res. Lett.*, **26 (8)**, 1019–1022.

Taylor, K. E., R. J. Stouffer, and G. A. Meehl, 2012: An overview of CMIP5 and the experiment design. *Bull. Amer. Meteor. Soc.*, **93 (4)**, 485–498, doi:10.1175/BAMS-D-11-00094.1.

Trenberth, K. E., 1999: Conceptual framework for changes of extremes of the hydrological cycle with climate change. *Wea. Clim. Extremes*, 327–339, doi:10.1007/978-94-015-9265-9_18.

Vecchi, G. A., and B. J. Soden, 2007: Global warming and the weakening of the tropical circulation. *J. Climate*, **20 (17)**, 4316–4340, doi:10.1175/JCLI4258.1.

Williams, I. N., R. T. Pierrehumbert, and M. Huber, 2009: Global warming, convective threshold and false thermostats. *Geophys. Res. Lett.*, **36 (21)**, doi:10.1029/2009GL039849.

Wodzicki, K., and A. Rapp, 2016: Long-term characterization of the Pacific ITCZ using TRMM, GPCP, and ERA-Interim. *J. Geophys. Res.*

LIST OF TABLES

TABLE 1. Initial parameter choices for the first model.

Variable	Value	Description
$\overline{T}$	287 K	Mean temperature
σ_T	16 K	Width of temperature dist.
$\overline{w}$	0	Mean vertical velocity, w
σ_w	1 mm s^{-1}	Width of w dist.

TABLE 2. The magnitude of fitted shift and increase modes along with their error (the magnitude of the response that the fitted shift-plus-increase fails to capture) for each of the experiments shown and discussed here. The precipitation response to a transient CO_2 increase in climate models is shown for the CMIP5 multi-model mean as well as for one GCM, MPI-ESM-LR, which is fit the best of all the CMIP5 models (see Pendergrass and Hartmann 2014b for details). The Model 1 experiments are shown in Fig. 4 and discussed in Section 2b-d. Model 2 experiments are shown in Figs. 6-8 and discussed in Section 3c.

Model	Experiment	Shift ($\%K^{-1}$)	Increase ($\%K^{-1}$)	Error (%)
CMIP5 MMM	$2xCO_2$	3.3	0.9	33
MPI-ESM-LR	$2xCO_2$	5.7	1.3	14
Model 1	Warm	7	7	2
	Weaken w	-4	-4	1
	Skew w	5	-1	27
	Warm, skew w	13	6	15
	Warm, weaken w, skew w	8	2	21
Model 2	Increase $\overline{Q}_n$, widen Q_n	11	9	11
	Increase $\overline{Q}_n$, decrease S	11	8	23
	Narrow Q_n, decrease S	0	-1	81
	Warm, increase S	0	0	22
	Warm, increase $\overline{Q}_n$	11	8	23
	Warm, narrow Q_n	0	-1	81
	Warm, GCM $\overline{Q}_n$, increase S	2.0	1.6	12
	Warm, GCM $\overline{Q}_n$, narrow Q_n	1.7	0.5	68

TABLE 3. Initial parameter choices for the second model.

Variable	Value	Description
$\overline{T}$	287 K	Mean temperature
σ_T	10 K	Width of temperature dist.
T_{max}	317 K	Cap on the temperature dist.
$\overline{Q}_n$	-88 W m^{-2}	Mean non-latent heating
σ_{Q_n}	2,500 W m^{-2}	Width of non-latent heating dist.
S	4.75×10^5 kg m^{-1} s^{-2}	Stability

TABLE 4. Standard deviation, skewness, and kurtosis of 500 hPa pressure vertical velocity from CMIP5 models and their response to warming (normalized by global mean surface temperature change).

Scenario	Model	std	Δstd	skew	Δskew	kurtosis	Δkurtosis
	($Pa\ s^{-1}$)	($\%K^{-1}$)		($\%K^{-1}$)		($\%K^{-1}$)	
RCP8.5	MIROC-ESM-CHEM	9.0	-2.5 %	-0.66	0.57%	5.8	0.85%
	FGOALS-g2	12	-2.7 %	-1.9	1.4 %	15	1.8 %
	NorESM1-M	8.1	-2.0 %	-1.2	1.4 %	8.6	3.5 %
	BNU-ESM	8.2	-2.1 %	-0.80	2.7 %	5.9	3.6 %
	CMCC-CESM	8.9	-1.9 %	-0.56	3.1 %	5.2	2.0 %
	BCC-CSM1.1	11	-0.97%	-1.8	4.0 %	15	6.3 %
	IPSL-CM5B-LR	11	-2.1 %	-3.3	4.4 %	48	5.8 %
	MPI-ESM-LR	11	-1.8 %	-1.00	4.6 %	7.4	4.8 %
	CNRM-CM5	11	-1.1 %	-1.9	5.4 %	20	8.3 %
	GFDL-CM3	8.5	-1.7 %	-1.4	6.2 %	13	10 %
	CCSM4	9.0	-1.4 %	-1.8	6.2 %	17	10 %
	GFDL-ESM2M	8.9	-1.4 %	-1.6	16 %	18	28 %
	IPSL-CM5A-LR	8.8	-1.2 %	-1.1	21 %	14	23 %
	GFDL-ESM2G	8.7	-1.1 %	-1.3	22 %	12	49 %
Transient CO_2 increase	IPSL-CM5B-LR	12	-2.1%	-3.2	2.3%	46	4.0%
	MIROC5	10	-2.0%	-1.4	4.4%	10	6.5%
	GFDL-ESM2G	8.8	-1.0%	-1.2	11 %	10	22 %
	IPSL-CM5A-MR	9.5	-2.1%	-1.4	14 %	18	19 %
	GFDL-ESM2M	8.9	-1.8%	-1.3	19 %	12	38 %
	IPSL-CM5A-LR	9.1	-2.7%	-0.86	27 %	11	26 %
Abrupt CO_2 increase	MIROC-ESM	9.3	-2.6 %	-0.65	0.29%	5.6	0.75%
	IPSL-CM5B-LR	12	-2.3 %	-3.3	3.0 %	48	5.1 %
	MIROC5	10	-1.9 %	-1.4	4.2 %	10	5.8 %
	CanESM2	9.3	-0.64%	-1.0	5.2 %	9.6	6.2 %
	MPI-ESM-LR	11	-1.4 %	-0.91	5.8 %	7.0	4.7 %
	MRI-CGCM3	11	0.84 %	-2.0	17 %	20	35 %
	IPSL-CM5A-MR	9.5	-1.0 %	-1.4	20 %	18	31 %
	IPSL-CM5A-LR	9.1	-1.4 %	-0.87	25 %	11	27 %

LIST OF FIGURES

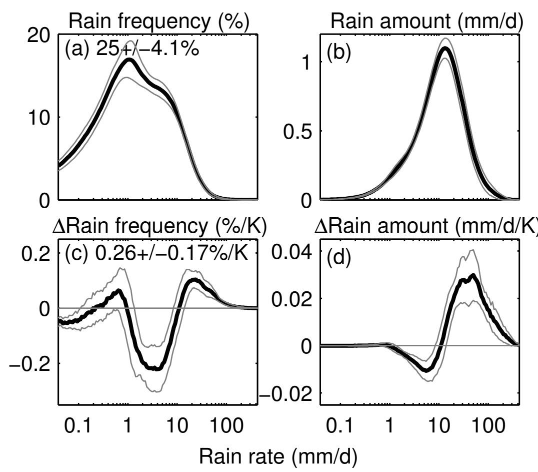

FIG. 1. The CMIP5 multi-model mean distributions of daily (a) rain frequency (with dry-day frequency at top left) and (b) rain amount, during the first ten years of the transient carbon dioxide increase emissions scenario, `1pctco2`. The response of (c) rain frequency and (d) rain amount to increasing carbon dioxide, calculated as the difference between the ten years at the time of carbon dioxide doubling and the first ten years and normalized by the change in global-mean surface temperature. Change in dry-day frequency ($\%\mathrm{K}^{-1}$) is noted in the top left corner of panel c. Error intervals are the 95% confidence limits according to a Student's *t*-test. As the distributions are plotted on a logarithmic scale, they are weighted by the rain rate *r* so that the area under the curve accurately represents the contribution of each rain rate to the total integral. Following Pendergrass and Hartmann (2014b and c), though the *r*-weighting is implicit to the procedure described there.

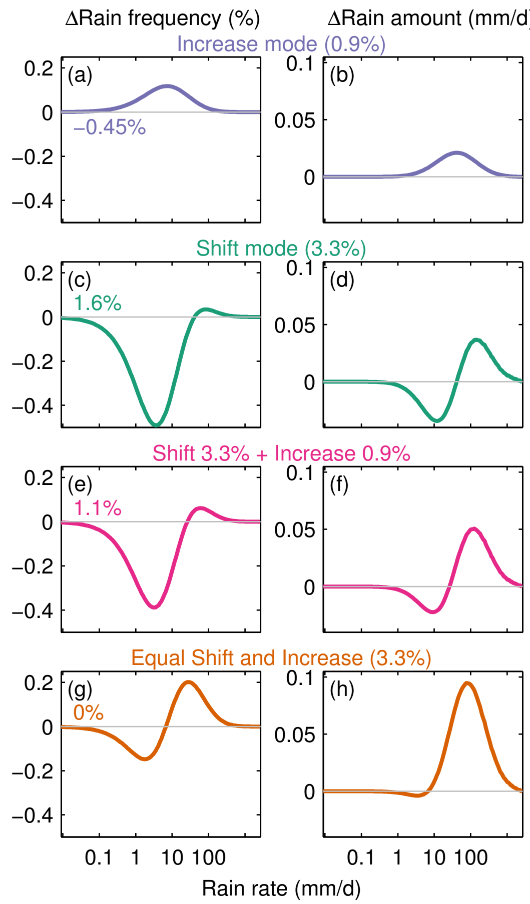

FIG. 2. The rain frequency (left) and amount (right) responses to (a-b, purple) an increase mode of 0.9%, (c-d, turquoise) a shift mode of 3.3%, (e-f, magenta) a shift mode of 3.3% and increase mode of 0.9%, and (g-h, orange) equal magnitude shift and increase of 3.3%. The color scheme corresponds to these modes throughout the paper. The initial distribution is shown in Fig 3.

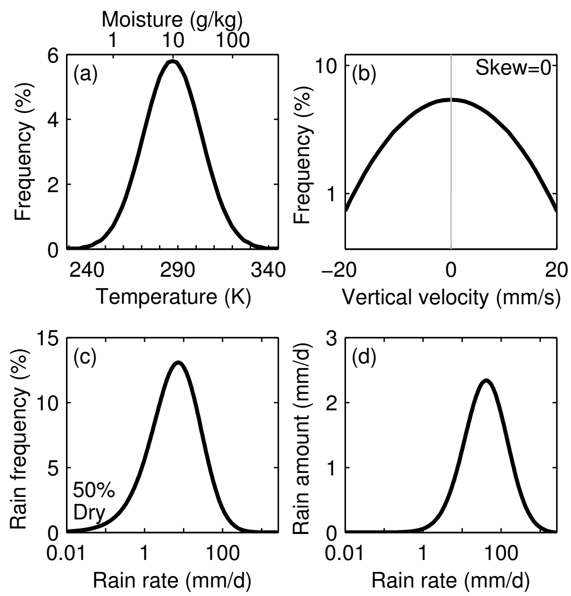

FIG. 3. The distributions driving the first model, where vertical velocity is prescribed: (a) temperature and moisture, and (b) vertical velocity (skewness is noted in the top right corner). The resulting distributions of (c) rain frequency (dry frequency, when rain rate is equal to zero, is noted in the bottom left corner) and (d) rain amount.

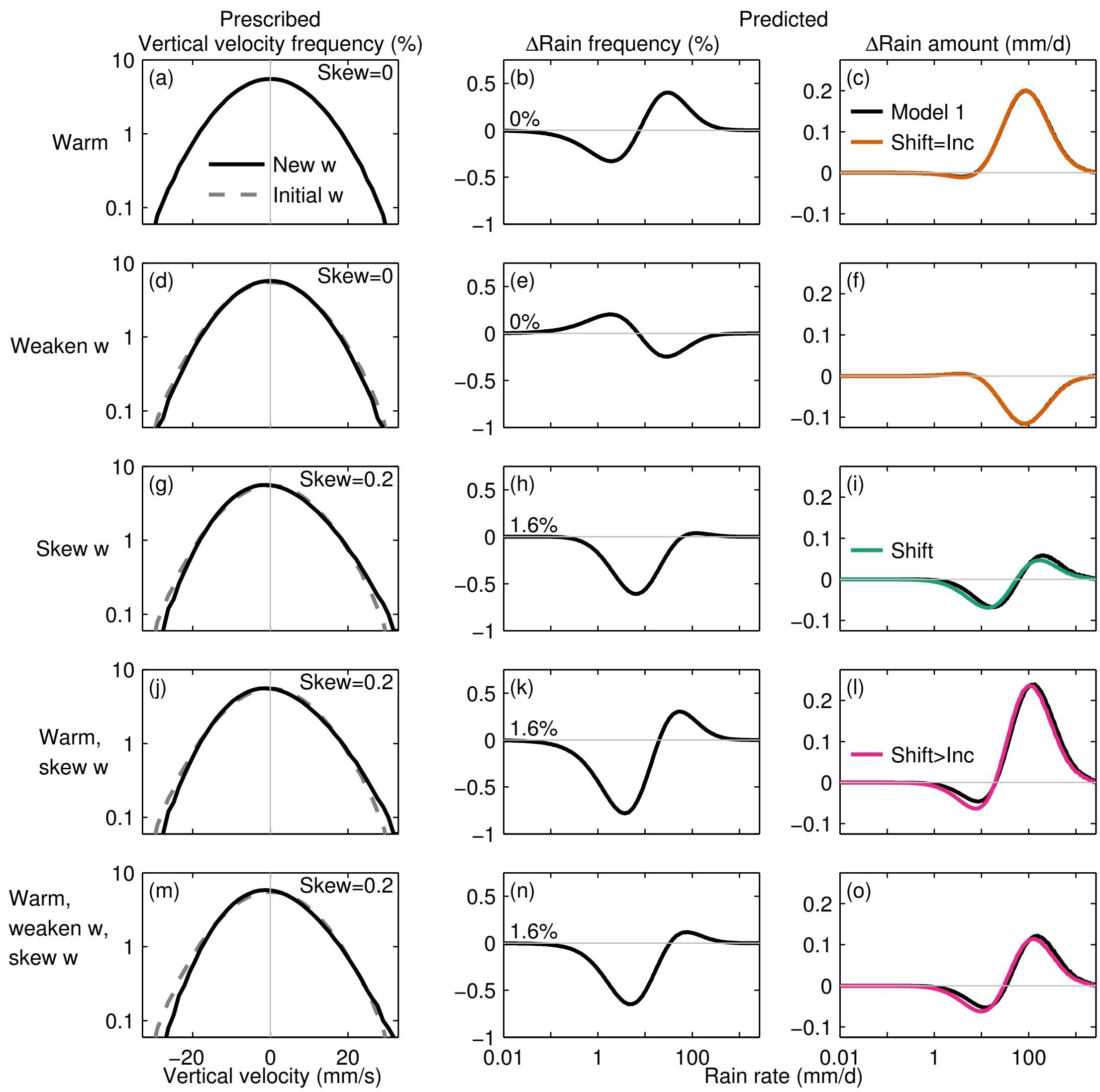

FIG. 4. Experiments with the first model. (left) Prescribed vertical velocity distribution, with the initial distribution in the gray-dashed line and each experiment's distribution in solid black (skewness noted at top right of each panel). (center) Predicted rain frequency response (change in dry frequency noted at center-left). (right) Predicted rain amount response in black, with the fitted shift-plus-increase response in color. Colors correspond to Fig. 2; the magnitude of the fitted shift and increase modes and their errors are listed in Table 2. Each row is one experiment: (a-c) warm, (d-f) weaken the vertical velocity distribution, (g-i) skew the vertical velocity distribution, (j-l) warm and skew, and (m-o) warm while weakening and skewing the vertical velocity distribution.

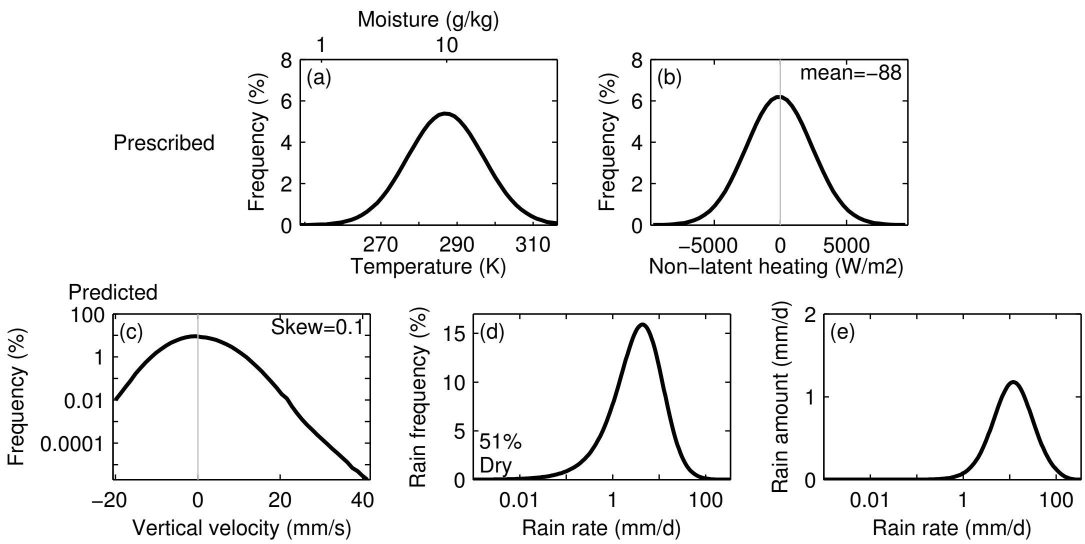

FIG. 5. The prescribed (top) distributions driving the second model, where vertical velocity is predicted: (a) temperature and moisture, and (b) non-latent heating (mean is noted in the top-right corner). The resulting predicted (bottom) distributions of (c) vertical velocity, (d) rain frequency (dry frequency noted in the bottom left corner) and (e) rain amount.

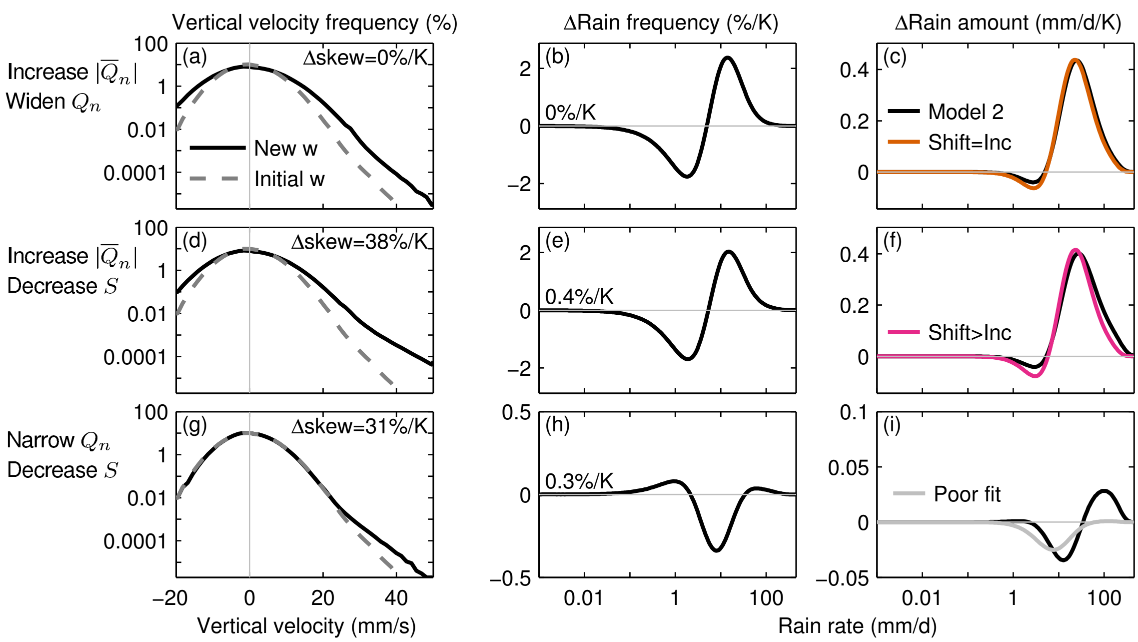

FIG. 6. Experiments varying parameters other than the mean temperature with the second model, following Fig. 4 but here the vertical velocity distribution (left) is predicted. (a-c) Increasing the magnitude of mean non-latent heating and increasing the width of the non-latent heating distributions, while holding all other parameters constant. (d-f) Increasing the magnitude of mean non-latent heating and decreasing stability. (g-i) Narrowing the non-latent heating distribution (decreasing σ_{Q_n}) and decreasing stability. Note the smaller y axis magnitudes in panels h and i. Changes are normalized by a 3 K warming for comparison with Figs. 7 and 8.

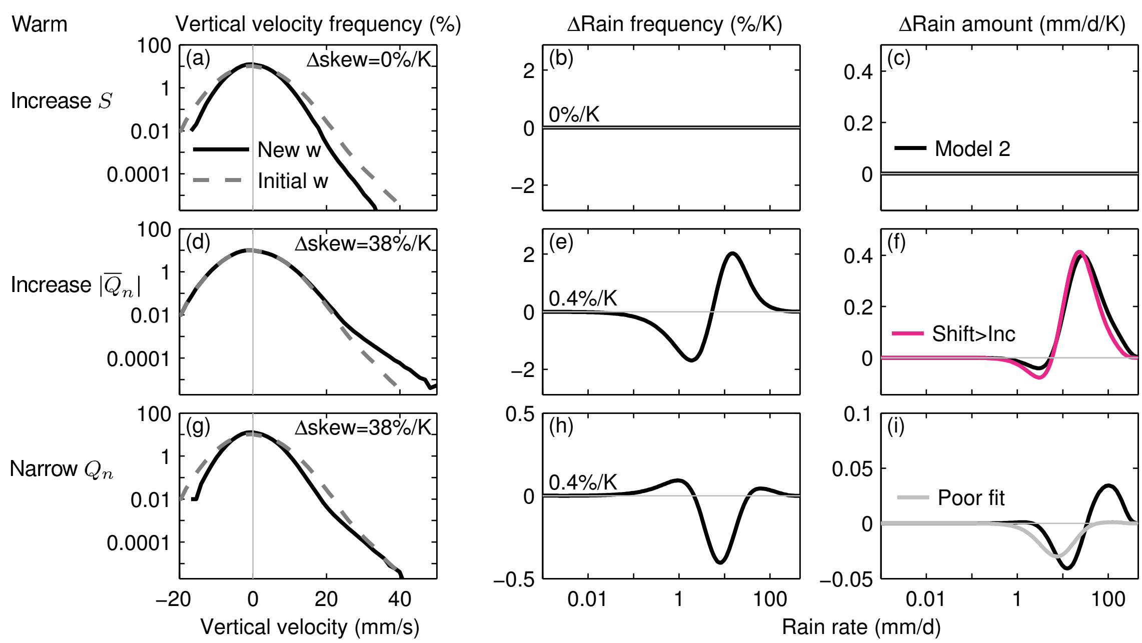

898 FIG. 7. Experiments warming while varying one other parameter with the second model, following Fig. 6: (a-c) increasing stability, (d-f) increasing the magnitude of mean non-latent heating, and (g-i) narrowing the non-latent heating distribution (decreasing σ_{Q_n}, note the smaller y axis magnitudes in panels h and i).

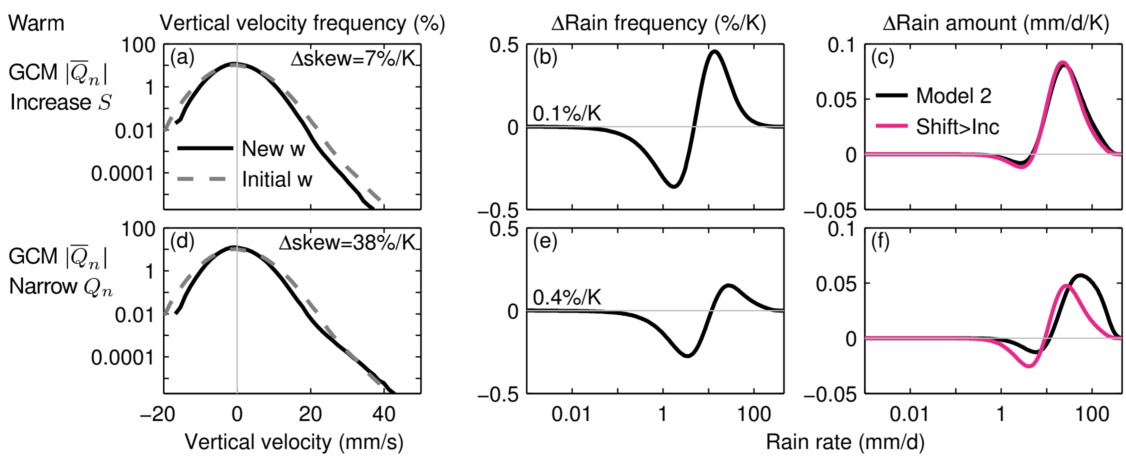

901 FIG. 8. Experiments warming, increasing the magnitude of the non-latent heating distribution by the value
902 from climate models, 1.1 W m^{-2} K^{-1}, while varying one other parameter with the second model, following
903 Fig. 6: (a-c) increasing stability, and (d-f) narrowing the non-latent heating distribution (decreasing σ_{Q_n}).

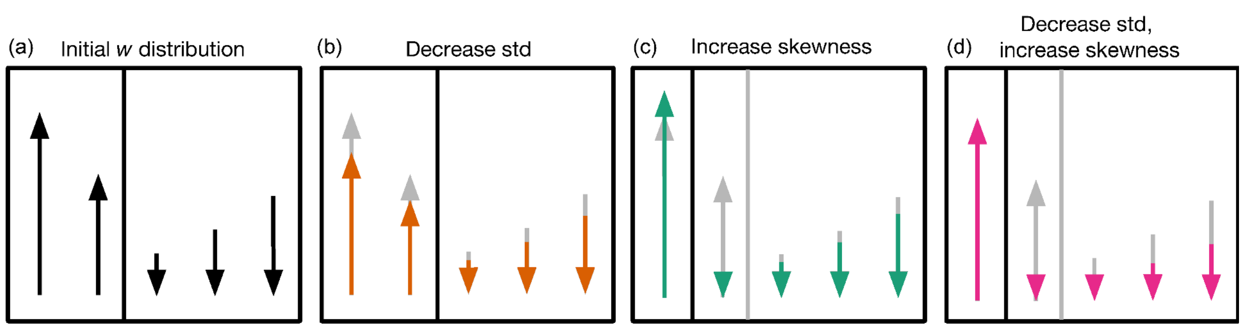

FIG. 9. A schematic showing the effects of changing width and skewness of the vertical velocity distribution. An initial skewed distribution of w (a), is perturbed by (b) decreasing its standard deviation, (c) increasing its skewness, and (d) both decreasing standard deviation and increasing skewness together.